Journal of Controlled Release 352 (2022) 61–73

Contents lists available at ScienceDirect

Journal of Controlled Release

journal homepage: www.elsevier.com/locate/jconrel

High-definition electroporation: Precise and efficient transfection on a microelectrode array

Bastien Duckert [a,b,*], Maarten Fauvart [b], Peter Goos [c,d], Tim Stakenborg [b], Liesbet Lagae [a,b], Dries Braeken [b]

[a] Department of Physics and Astronomy, KU Leuven, Celestijnenlaan 200d, 3001, Leuven, Belgium
[b] imec, Kapeldreef 75, 3001, Leuven, Belgium
[c] Department of Biosystems, KU Leuven, Willem de Croylaan 42, 3001, Leuven, Belgium
[d] Department of Engineering Management, University of Antwerp, Prinsstraat 13, 2000, Antwerp, Belgium

ARTICLE INFO

Keywords:
CMOS microelectrode arrays
High-definition electroporation
Intracellular delivery
Single-cell transfection
Spatially-resolved multiplexing
Primary cells
RNA delivery
Design of experiments
Dosage control

ABSTRACT

Intracellular delivery is critical for a plethora of biomedical applications, including mRNA transfection and gene editing. High transfection efficiency and low cytotoxicity, however, are often beyond the capabilities of bulk techniques and synonymous with extensive empirical optimization. Moreover, bulk techniques are not amenable to large screening applications. Here, we propose an expeditious workflow for achieving optimal electroporation-based intracellular delivery. Using the multiplexing ability of a high-definition microelectrode array (MEA) chip, we performed a sequence of carefully designed experiments, multiple linear regression modelling and validation to obtain optimal conditions for on-chip electroporation of primary fibroblasts. Five electric pulse parameters were varied to generate 32 different electroporation conditions. The effect of the parameters on cytotoxicity and intracellular delivery could be evaluated with just two experiments. Most successful electroporation conditions resulted in no cell death, highlighting the low cytotoxicity of on-chip electroporation. The resulting delivery models were then used to achieve dosage-controlled delivery of small molecules, delivery of Cas9-GFP single-guide RNA complexes and transfection with an mCherry-encoding mRNA, resulting in previously unreported high-efficiency, single-cell transfection on MEAs: cells expressed mCherry on 81% of the actuated electrodes, underscoring the vast potential of CMOS MEA technology for the transfection of primary cells.

1. Introduction

Electroporation has become the most prominent physical transfection method thanks to high delivery success rates and convenient implementation [1]. During electroporation, cells are subjected to an electrical field that forces transient pores in the plasma membrane. These pores allow for the entry of molecules from the extracellular medium, which get trapped in the cell cytosol after the pores reseal.

In the simplest implementation of electroporation, a suspension of cells is mixed with the cargo in a cuvette fitted with two large electrode plates. Then, high-voltage pulses (up to thousands of volts) are applied between the plates [2,3]. Electroporation in bulk, however, results in high cytotoxicity. Overexposure to the heterogeneous electric fields in the cuvette, Joule heating, and release of metallic ions from the electrodes can negatively impact cell viability. The cells that do survive the process can suffer from an altered biological function, e.g. disrupted gene expression profiles in T cells, limiting the use in manufacturing of cell immunotherapies [4,5]. Optimization of electroporation conditions for a given cell and cargo type relies on the interaction of a large set of parameters and, traditionally, researchers have defaulted to lengthy, one-factor-at-a-time screening experiments to study electroporation [6–10].

Commercial transfection technologies often are “one size fits most” products, optimized for the delivery of nucleic acids in immortalized cell lines or a few primary cell types [11], as they often struggle with “hard-to-transfect” cells and non-nucleic acid cargos. For instance, commercial electroporators (i.e. Neon™ transfection system) can reach cell viabilities and transfection efficiencies above 90% when applied to well established cell lines, but both figures of merit drop close to 60% when targeting primary cells. Recently, technologies based on physical

* Corresponding author at: Department of Physics and Astronomy, KU Leuven, Celestijnenlaan 200d, 3001, Leuven, Belgium.
E-mail addresses: bastien.duckert@imec.be (B. Duckert), maarten.fauvart@imec.be (M. Fauvart), peter.goos@kuleuven.be (P. Goos), tim.stakenborg@imec.be (T. Stakenborg), liesbet.lagae@imec.be (L. Lagae), dries.braeken@imec.be (D. Braeken).

https://doi.org/10.1016/j.jconrel.2022.10.001
Received 30 May 2022; Received in revised form 14 September 2022; Accepted 1 October 2022
Available online 18 October 2022

membrane disruption applied at the single-cell level have appeared to fill in this need for a cell type and cargo agnostic intracellular delivery method [12]. The localized membrane disruption created by those techniques can result in viabilities above 90% in primary cells, with efficiencies upward 80% with single-cell addressability, and they have been reported to minimally disrupt cell function compared to bulk methods [13,14].

Planar Microelectrode Arrays (MEAs) are used for electrical recording and stimulation of cells grown on their surface and, when applied to electroporation, offer improved control over cell exposure to electric fields, which should limit cytotoxicity. Recently, we demonstrated a MEA chip fabricated using complementary metal oxide semiconductor technology (CMOS) featuring over 16,000 individually addressable and densely packed (>4000 electrodes/mm^2) microelectrodes (Fig. 1A and B). This device has been used for the label-free monitoring of single cells through recording of electrical activity and impedance measurements in vitro [15,16]. Here, we focus on the MEA's precise electrical stimulation capability to electroporate human dermal fibroblasts for the intracellular delivery of multiple molecule types with exquisite efficiency. The subcellular size of the electrodes (down to 8.75 μm^2), the close distance between them and the ability to address them individually permits single-cell electroporation with an unprecedented spatiotemporal resolution (Fig. 1C), a process we coin high-definition electroporation (HD-EP).

After preliminary experiments that showcased the HD-EP chip's ability to precisely deliver different molecules in HeLa cells with a high success rate (Supplementary Fig. S1), we set out to optimize the electroporation of primary cells and maximize the quantity of molecules delivered. Importantly, individual control over each electrode enables an exceptional multiplexing ability that we exploit through highly parallelized screening experiments following the principles of Design of Experiments (DoE), culminating in a workflow that yields very efficient on-chip electroporation, cargo delivery, and transfection with high cell viability (Fig. 1D). Five electroporation parameters were included in the screening experiment: pulse amplitude, duration, number, symmetry, and electrode size were varied to generate 32 distinct electroporation conditions. Each condition has been tested twice in two separate, highly parallelized experiments. We measured the degree of electroporation on the one hand, quantified as the average cell fluorescence intensity after delivery of a small fluorescein-labelled dextran (10 kDa), and cell survival on the other hand. Multiple linear regression models were then used to map the relationship between the programmed voltage pulse parameters and the degree of electroporation and cell death. Next, the dextran delivery model was validated by predicting the outcome of three arbitrary, untested electroporation pulse programs, showcasing dosage-controlled delivery. Finally, we used the obtained on-chip electroporation regression model to design electroporation conditions to maximize electroporation and cell survival, for the delivery of a 70-kDa dextran, Cas9-GFP single-guide RNA ribonucleoprotein complexes (RNP, over 200 kDa), and an mCherry-encoding mRNA (1 kb). Finally, we also discuss which application could be enabled by HD-EP in the future.

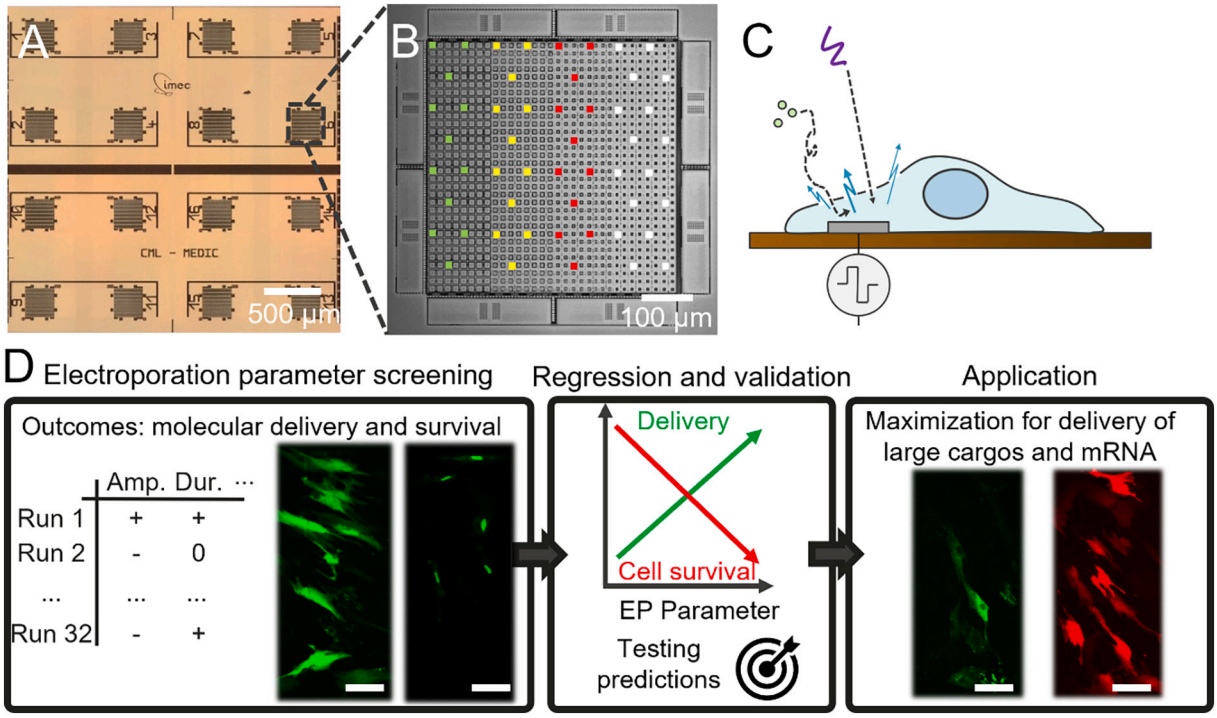

Fig. 1. Overview of electroporation on the CMOS HD-EP chip and the workflow proposed in this study. A: Image of the electrode area of the CMOS HD-EP chip with 16 electrodes clusters, each containing 1024 individually addressable microelectrodes. B: Confocal microscopy close-up view of an electrode cluster. The 1024 TiN electrodes are split in four different blocks of different electrode sizes. For this work, each electrode cluster has been divided into four different experimental compartments corresponding to areas with different electrode sizes. The colored squares represent electrodes selected to submit an electroporation pulse train, and the different colors represent different electroporation conditions. C: Conceptual drawing of electroporation on chip. Electrical pulses are submitted through an electrode to create pores in the membrane of the cell adhering to it to deliver small molecules or nucleic acids. D: Electroporation workflow: 32 different electroporation conditions designed with DoE can be applied to different areas of the HD-EP chip (Amp.: Amplitude; Dur.: Duration). Each electroporation condition was applied for the electroporation of primary human dermal fibroblasts grown on the chip, and we measured the intracellular delivery of a small fluorescein-labelled dextran (left) and the extent of cell survival (right) with confocal microscopy. Multiple linear regression models were then used to map the relationship between those outcomes and the pulse parameters, and the predictions of the dextran delivery model were experimentally validated. Finally, we used the regression models to design electroporation conditions that would maximize electroporation and cell survival and applied them to the delivery of a Cas9-sized dextran (70 kDa) (in green) and an mCherry-encoding mRNA (1 kb) (in red). Scale bar is 100 μm. (For interpretation of the references to colour in this figure legend, the reader is referred to the web version of this article.)

2. Results and discussion

2.1. Highly multiplexed parameter screening for on-chip electroporation

We first assessed electroporation on the HD-EP chip by growing primary human dermal fibroblasts for approximately 30 h and then electroporating them in the presence of a fluorescein-labelled dextran ("FD10"; 10 kDa). Each electrode cluster was divided into four regions of different electrode sizes organized in a non-overlapping pattern, and distinct electroporation conditions were applied to sets of 12 to 16 active electrodes per region (one condition per electrode size) (Fig. 2A). The spatially resolved pattern of electroporation is detailed in the Materials and Methods (Fig. 8D). For each of the 32 different electroporation conditions tested, the fluorescein intensity of the cells post-electroporation was measured to quantify intracellular FD10 delivery. Single-cell electroporation with the HD-EP chip is visible by combining cell nuclei staining (SYTO 61, red, Fig. 2B) with FD10 delivery (green, Fig. 2C).

Most microelectrodes are in contact with a single cell, while neighbouring cells, even those situated in the small space between active electrodes, were left unstimulated and thus did not take up FD10 (Fig. 2C). The ability to target single cells, however, was found to be dependent on electrode size and decreased on larger electrodes. The largest electrodes on the HD-EP chip (11 × 11 μm^2) were often in contact with more than one cell at a time (Fig. 2D, white arrows), while electrodes sized 7 × 6.5 μm^2 and smaller delivered the dye in single cells most of the time (in Fig. 2D, five of the largest electrodes are in contact with two or more fluorescent cells at a time (42%), while none of the smaller electrodes displayed are touching more than one fluorescent cell). When observing all the electrodes used for the screening experiment, 48% of the 11 × 11 μm^2 electrodes, 84% of the 7 × 6.5 μm^2 electrodes, 81% of the 4.5 × 4.5 μm^2 and 84% of the 2.5 × 3.5 μm^2 electrodes resulted in single-cell electroporation, respectively. A higher degree of single-cell addressability would be achievable, however, if the electrode selection was based purely on cell location.

Out of 32 runs in the screening experiment, 13 did not result in measurable FD10 intensity (41%). Of those runs, 11 were performed at the lowest level of pulse amplitudes (0.585 V peak-to-peak). While electroporation at those low voltages resulted in uptake of propidium iodide in the cell death analysis experiment, the 585 mV pulses submitted to the electrodes may not have created pores large enough for the passage of dextran into the cells, even at the highest pulse number.

2.2. Regression model fitting to FD10 delivery

For each run, the average fluorescence intensities of cells located on

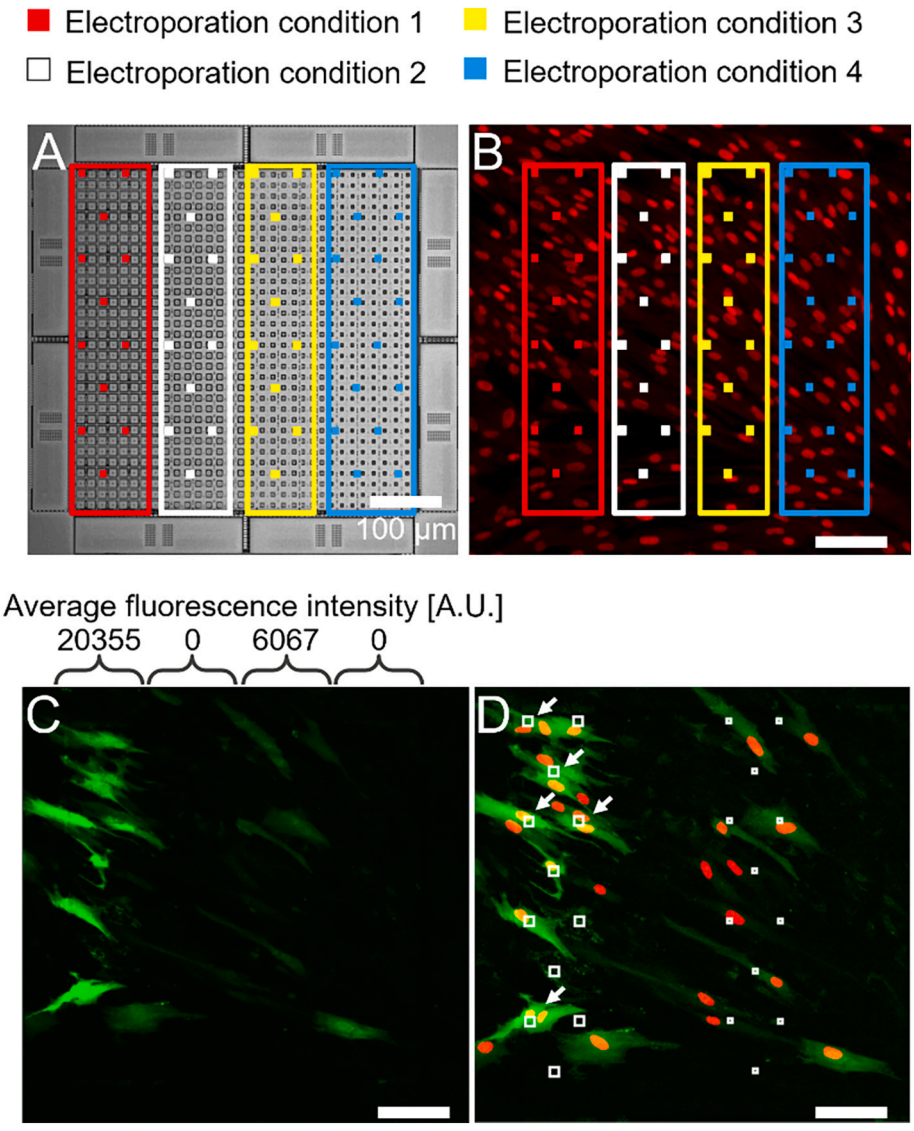

Fig. 2. Dextran delivery screening experiment. A: The electrode cluster has been separated in four different regions, each used to submit a distinct electroporation pulse to the cells grown on the chip. The colored rectangles outline the different regions, and the colored squares indicate the 12 to 16 electrodes that have been activated during electroporation. Each region comprises electrodes of different sizes. B: Nuclei of the cells, showing that cells are covering the entire cluster of electrodes, and that cells were present in between activated electrodes. C: Imaging of the dextran delivered in cells after electroporation. Cells electroporated with different electroporation conditions resulted in distinct average fluorescence intensity. The electroporation conditions 1 and 3 have resulted in average cell fluorescence intensities of 20,355 and 6067 A.U., respectively, while 2 and 4 have not resulted in detectable uptake of dextran. Green: fluorescein-labelled dextran; Red: SYTO 61 nucleus staining. D: To show that most electrodes electroporated a single cell, the nuclei of the electroporated cells (red) and outlines of the active electrodes for conditions 1 and 3 are overlayed on the dextran image. The contrast of the dextran image has been locally altered to better show cells of low fluorescence intensity. (For interpretation of the references to colour in this figure legend, the reader is referred to the web version of this article.)

an active electrode was measured, and the data collected was used to build a multiple linear regression model (data in Supplementary Materials) comprising the main effects of all the parameters, their interactions and the quadratic effects of the four quantitative parameters. A blocking factor representing the possible variations in results between chips was also included. This full model thus contains 21 terms: an intercept, a blocking factor, 5 main effects, 4 quadratic effects and 10 interactions. Tables with all the terms of the model and detailed explanations are available in Materials and Methods and in Fig. 8A and B. Not all those terms, however, have a significant effect within the model. Two different, reduced, models were generated with backward stepwise regression by minimizing either the corrected Akaike Information Criterion (AICc) or the Bayesian Information Criterion (BIC). These are routine model selection criteria used when the number of observations is large compared to the number of terms to estimate. They were preferred over the usual *p*-value evaluation as that method, when applied to large datasets, usually results in most terms being significant and in an overfitting model [17]. A summary of the statistical properties for both models is provided in Fig. 3A. The BIC model shows the highest coefficient of determination (R^2) and adjusted coefficient of determination (aR^2), at the cost of increased complexity as seen in the larger number of terms in the model. While simpler models should be preferred to mitigate the risks of overfitting the sample data, the similar predicted residual error sum of squares (PRESS value) of the BIC model indicates that it does not present more risks of overfitting. For those reasons, the BIC model was selected to optimize electroporation on chip. Fig. 3B and C display an analysis of variance and a comparison of its predictions to the experimental data.

Fig. 4A shows the relationship between the average cell fluorescence intensity and the electroporation parameters. A summary of all the factors present in the model can be seen in Fig. 4B. The estimates of the factors indicate the importance that each factor has within the model, as higher absolute values show larger impact within the model. The lack of significance of the blocking factor suggests that there was no difference in fabrication or handling between the two chips used in parallel, and that the results obtained between them are not statistically different. A detailed and interactive report of this dextran delivery model is available in the Supplementary materials.

The two terms with the highest impact in the model, as seen by highest estimates, are the amplitude and the duration of the pulse (Fig. 4B). This is consistent with previous theoretical and experimental work on electroporation [1], in which pulse amplitude and duration were found to work through distinct mechanisms. A strong pulse will initially create more, but smaller pores, while sustaining the pulse over time will expand the pores [18]. In addition to their main effects, the pulse amplitude and duration contribute to the model with a strong positive interaction. The Amplitude*Duration interaction term may not only result from the synergy between the two parameters during pore formation and expansion, but also through the appearance of electrochemical reactions when voltages above ca. 1 V are applied to titanium nitride electrodes [19,20]. Below that voltage threshold, only short capacitive currents can be submitted through the electrodes and the pulse duration has no effect. Above that threshold, however, longer, faradaic currents can be sustained, and the pulse duration develops a strong effect within the model (Fig. 4C).

Electrode size, the pulse symmetry and the higher order terms involving them have a slightly milder impact in the model. Symmetric pulses were more effective than asymmetric pulses. In an asymmetric pulse, the longer but weaker phase might only slightly increase the transmembrane potential or might not be able to sustain long faradaic currents, resulting in short and ineffective capacitive pulses. The presence of an interaction term involving the pulse amplitude and symmetry hints at that hypothesis. Because our HD-EP chip can only submit trains of short square pulses, asymmetric pulses have been introduced in the screening experiment to emulate the "double pulse electroporation" [6] strategy used in commercial electroporators, which has been shown to improve delivery efficiency by electrophoretically driving charged molecules in the cells. We hypothesized that the stronger positive phase might create a net faradaic current that would attract negatively charged molecules like the fluorescein-labelled dextrans, while the weaker negative phase would only generate a short capacitive current that would not contribute to the net movement of charges near the electrodes. That did not seem to occur, however.

The negative, quadratic effect of electrode size gives an inverted parabolic profile to the fluorescence intensity curve: the smallest and the largest electrodes used in the screening experiments resulted in lower fluorescence intensities than electrodes of intermediate sizes (Fig. 4A). The model suggests an optimal electrode size of approximately 80 μm^2 for the cells used in this study. This may be caused by two opposite effects. The area of electroporated cell membrane scales with electrode size, and larger electrodes create more pores overall, but larger electrodes create the risk of partial contact with the cells, and current emitted by large electrodes may be dissipated through electrode surface that is not covered by cells.

Finally, the pulse number seems to have a very limited effect on the delivery of dextran. The quadratic effect of the pulse number is significant, while the main effect of the pulse number is not. The model predicts that increasing the number of pulses is effective only in the case of

A

Comparison of selected models						
Criterion	# Terms	R^2	aR^2	PRESS	AICc	BIC
minimum AICc	7	0.65	0.57	0.41	638.69	644.16
minimum BIC	11	0.79	0.7	0.436	640.04	641.21

B

BIC model, Analysis of Variance					
Source	DF	Sum of Squares	Mean Square	F Ratio	Prob > F
Model	10	990929328	99092933	8.0852	<.0001
Error	21	257379456	12256165		
C. Total	31	1248308783			

C

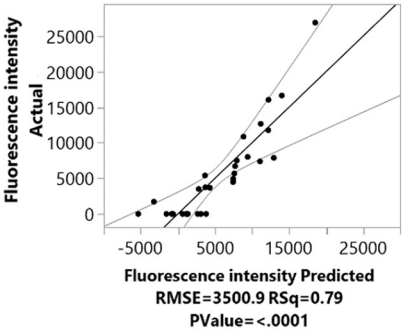

Fig. 3. Model selection for the dextran delivery screening experiment. A: Statistical properties of the two different models generated through stepwise regression. The BIC model shows higher R,^{2} aR^2 and PRESS, so was selected as the model used to fit the dextran delivery data. B: Analysis of Variance table of the BIC model. DF: Degrees of Freedom. C: Actual Fluorescence intensity, obtained experimentally, vs the Fluorescence intensity predicted by the BIC model. The dashed curves represent the 0.05 significance curves. RMSE: Root-mean-square error.

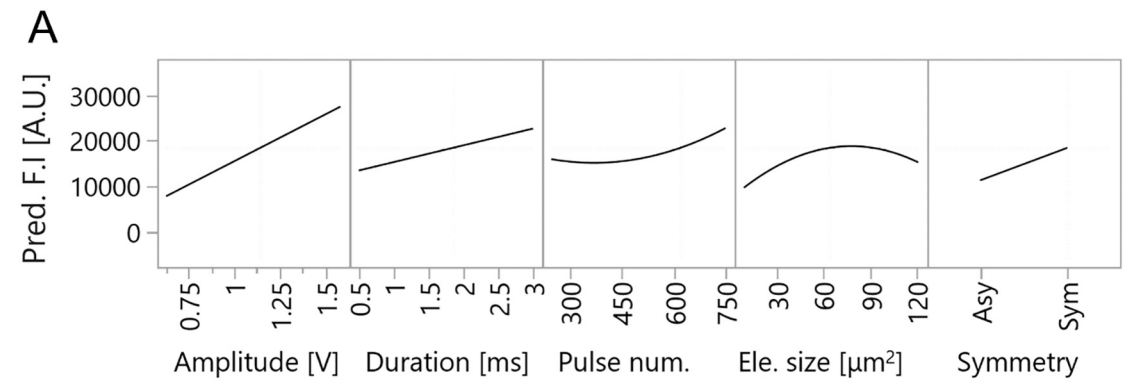

B

Term	Estimate	Std Error	t Ratio	Prob>|t|
Intercept	11695	1608	7.27	<.0001*
Amplitude(0.585,1.54)	7737	1239	6.24	<.0001*
Amplitude*Duration	4778	1449	3.30	0.0034*
Duration(0.5,3)	3834	1038	3.69	0.0013*
Pulse number*Pulse number	3378	1579	2.14	0.0443*
Electrode size(8.75,121)	2808	822	3.41	0.0026*
Pulse number(250,750)	1541	995	1.55	0.1365
Amplitude*Symmetry[Asy]	-1797	895	-2.01	0.0576
Pulse number*Symmetry[Asy]	-1906	907	-2.10	0.0480*
Symmetry[Asy]	-2378	666	-3.57	0.0018*
Electrode size*Electrode size	-6072	1785	-3.40	0.0027*

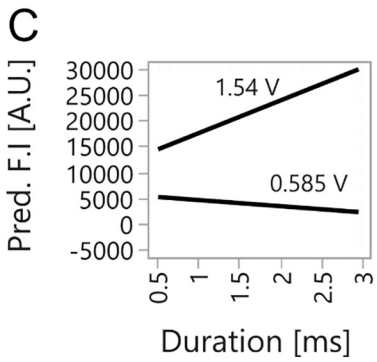

Fig. 4. Relationship between the parameters and the electroporation of cells on the HD-EP chip. A: Relationship between the electroporation parameters and the predicted average fluorescence intensity of the cells after electroporation in presence of FD10 when the parameters are set at their middle level, and Symmetry is set as Sym. B: Sorted estimates of the factor effects present in the model. Varying factors that have a higher scaled estimate has more impact on the predicted fluorescence intensity than varying factors with lower scaled estimates. C: Interaction between the pulse Duration and the pulse Amplitude when the other factors are set at their middle level, and Symmetry is set as Sym. The effect of Duration depends on the level of the pulse amplitude: it is non-existent at the lowest amplitude and becomes more pronounced as the amplitude is increased. The top curve shows the predictions for a high pulse amplitude and the bottom line shows predictions for a low amplitude, which correspond to the faradaic and capacitive regimes, respectively. A detailed and interactive model is available in the supplementary materials.

>500 symmetric pulses (visible in the interactive report available in the Supplementary materials). This dependency is present in the model in the form of a Pulse Number*Symmetry interaction term and could be explained this way: increasing the pulse number can be seen as a means to increase the time during which the cell membrane experiences an electric field. That is why increasing the pulse number may contribute to stabilize or expand the electropores formed by the initial pulses, effectively widening the time window available for the entry of molecules in the cells, while also prolongating electrophoretic delivery of molecules [21]. The range of pulse numbers evaluated in this study, however, may not have been wide enough and extending the range of pulse numbers tested may result in a more drastic effect within the model, even for asymmetric pulses.

2.3. Validation of the regression model and dosage-controlled delivery

To verify the model's ability to predict the fluorescence intensity of cells electroporated with previously untested sets of parameters, we performed a validation experiment. Three electroporation conditions were designed to deliver enough FD10 in cells to reach fluorescence intensities of 5000 A.U., 10,000 A.U. and 15,000 A.U, which are values expected within the range of fluorescence uptake after EP. The three different electroporation conditions were tested simultaneously in the same electrode cluster. In total, four replicates were performed on the electrode clusters on a single chip. The values of the parameters tested, and the confidence intervals of the predicted fluorescence values are shown in Fig. 5A.

Fig. 5B and C show fluorescence microscopy images resulting from two replicates, while Fig. 5D shows the average fluorescence of the cells for all four replicates. The fluorescence intensities of the cells electroporated during the validation experiment are mostly in agreement with the predictions of the model, and we conclude that the model can be used to define electroporation conditions that would optimize the delivery of small molecules. Out of twelve different trials, only three resulted in average fluorescence intensities that were outside of the prediction intervals (Fig. 5D, dashed lines). Experimentally validating the regression model built on a designed screening experiment corroborates that DoE is a quick and reliable way to navigate the electroporation parameter space. Moreover, the ability to tailor the electroporation conditions to introduce a desired quantity of molecules in the cells implies a dosage-controlled intracellular delivery.

The standard deviation values associated with the mean intensities (Supplementary Fig. S2), however, reflects the large variability between cells electroporated under similar conditions. For instance, in Fig. 5C, a red arrow shows a surprisingly bright cell, compared to its dim neighbours. We have identified three main reasons explaining this variability, all originating from the random shape and location of the cells on the HD-EP chip. i) Cells may not always fully cover an electrode. The variable contact area between the two may result in different electroporation outcomes, such as electroporation of a smaller patch of membrane, or electrical current lost through the uncovered electrode area rather than passing through the cells. ii) Cells can cover multiple active electrodes at the same time and are more electroporated than intended. Similarly, the fibroblasts investigated in this study sometimes spanned between two compartments and may have been electroporated twice with different parameters (Fig. 5B and C, white arrows). iii) Variability in cell size generates variability in fluorescence intensity. The brightness of a cell is related to the intracellular concentration of fluorophores rather than an absolute number of molecules. For the same quantity of fluorophores diluted within the cytosol of two cells, a larger cell will appear fainter than a smaller cell. While the erratic shapes of fibroblasts complicated the measurements, we predict that cell brightness should be

A

Predicted F.I [C.I.]	Amplitude [V]	Duration [ms]	Pulse number	Electrode size [μm²]	Symmetry
15000 [11334,18682]	1.22	1.55	600	121	Symmetric
10000 [6883, 13134]	1.01	1.25	500	45.5	Symmetric
5000 [2171, 7893]	1.12	0.82	400	20.25	Symmetric

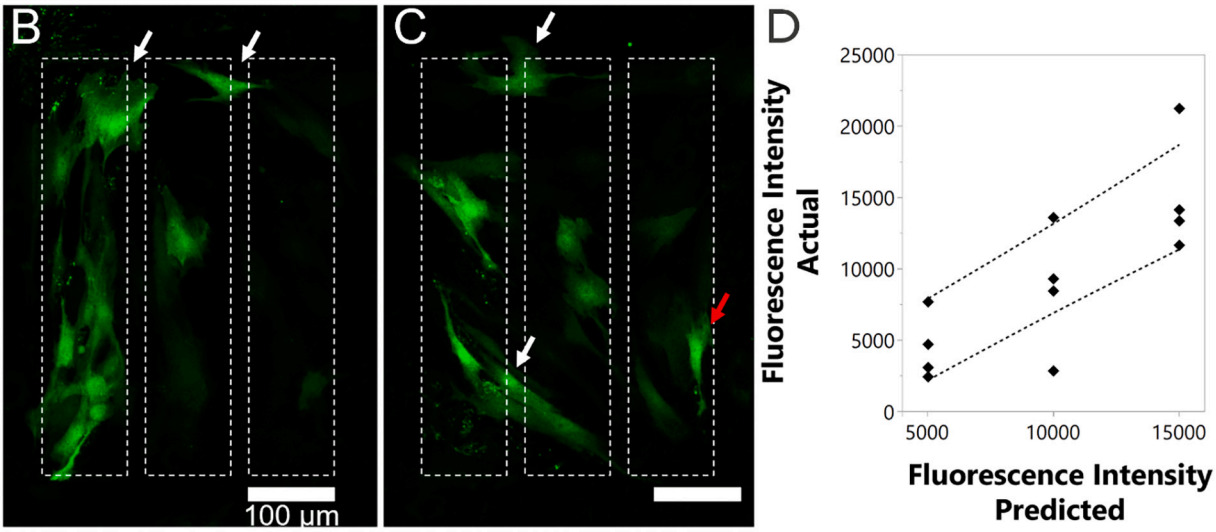

Fig. 5. Validation of the dextran delivery model. A: Values of the electroporation parameters predicted to achieve high, medium, and low fluorescence intensities (15,000 A.U., 10,000 A.U. and 5000 A.U, respectively), and the associated confidence intervals (C.I.). B and C: Confocal fluorescence microscopy of FD10 delivered in cells in two different replicates. The dashed rectangles correspond to different experimental compartments, as for the screening experiment (Fig. 2A). The aim was to generate bright cells in the left compartment, medium intensity cells in the middle, and dim cells in the right compartment. The white arrows point to cells spanning multiple compartments, and the red arrow points to an abnormally bright cell, showcasing the cell-to-cell variability in fluorescence intensity. D: Actual average fluorescence intensity of the cells after electroporation with the validation parameters vs the values predicted by the model. The dashed bars represent the 95% prediction interval. In 9 cases out of 12, the experimental values were in agreement with the model. (For interpretation of the references to colour in this figure legend, the reader is referred to the web version of this article.)

inversely proportional to cell size, which will be verified in a follow-up study.

2.4. Cell survival analysis and fitting

The 32-run screening experiment was then adapted to observe the extent of cell death. To distinguish the cells that were electroporated from the ones that were left unaffected, electroporation was performed in the presence of Propidium Iodide (PI), a cell impermeant red nucleic acid stain. After giving ten minutes for the cells to recover, they were stained with YO-PRO-1, a green apoptosis and cell death stain. Fig. 6D and E show the results of a run where surviving cells display only red fluorescence (white arrows), while cells that died from electroporation display both red and green fluorescence (green arrows). Only six out of the 32 runs resulted in identifiable cell death, most likely because the range of values selected for the screening experiment were designed to avoid ubiquitous cell death and subsequent detachment from the chip surface (details in the Materials and Methods).

The cell survival rate was then calculated from the ratio of dead or dying cells to electroporated cells. That value varied between 62% and 100%. The data gathered for each run was then used to build a regression model to describe cell survival in terms of the electroporation parameters and two different models were generated in the same manner as in the previous screening experiment. Both models showed comparable coefficients of determination and like in the previous case, BIC minimization resulted in a more complex model than AICc minimization. The BIC model, however, presented a possible sign of overfitting: the pulse number appeared to have a significant quadratic effect within the BIC model, but with minimal impact on the predicted cell survival. Removing the pulse number (main and quadratic effects) from the BIC model yielded the AICc model. That is why the AICc model was favoured to find optimal electroporation parameters. Fig. 6 details this model and its parameters. A detailed and interactive report of the model is available in the Supplementary Materials.

The significant parameters contained in this model are the pulse amplitude, the pulse symmetry, and the electrode size (Fig. 6F). In agreement with previous reports, cell survival decreases quadratically with the pulse amplitude [6] (Fig. 6F and G). Symmetric pulses showed more toxicity than asymmetric pulses, most likely for the same reasons they were more effective in delivering the FD10. Finally, larger electrodes result in increased cell death, while keeping the other pulse parameters constant. Electroporation on large electrodes may cause the disruption of a larger patch of cell membrane, resulting in unrepairable membrane damage or lethal loss of intracellular components. Conversely, electroporation on smaller electrodes guarantees cells survival, in agreement with previous reports that localized membrane poration only minimally disrupts cells viability and function [13,14].

This model fitted to the cell survival data, however, lacks some of the significant terms present in the dextran delivery model. For instance, the duration and number of pulses were not found to have a significant

A

Statistical properties of the cell survival model						
Criterion	# Terms	R^2	aR^2	PRESS	AICc	BIC
minimum AICc	7	0.79	0.74	0.615	-99.1	-93.7

B

Cell survival model, Analysis of Variance					
Source	DF	Sum of Squares	Mean Square	F Ratio	Prob > F
Model	6	0.15915496	0.026526	15.7146	<.0001
Error	25	0.04219929	0.001688		
C. Total	31	0.20135425			

C

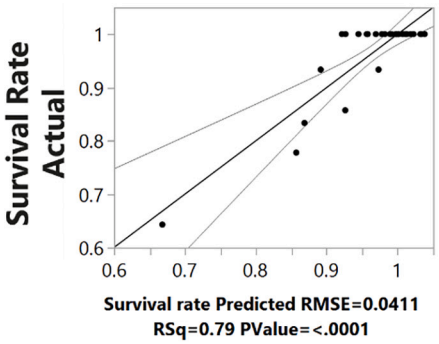

D

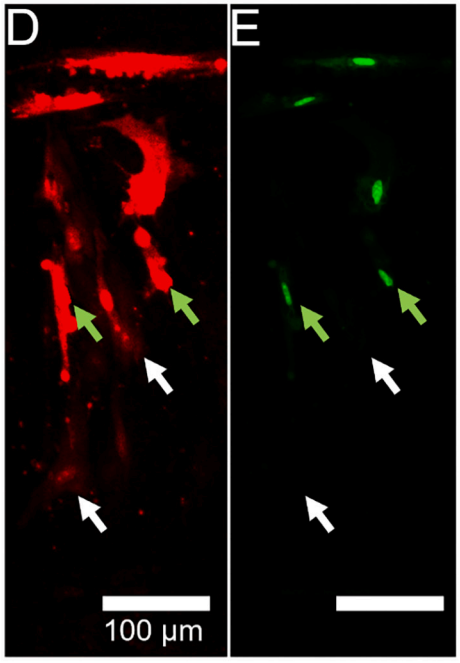

E

F

Term	Estimate	Std Error	t Ratio	Prob>|t|
Intercept	0.968	0.0116	83.23	<.0001*
Amplitude x Symmetry[Asy]	0.030	0.0105	2.86	0.0084*
Symmetry[Asy]	0.020	0.0076	2.67	0.0130*
Electrode size	-0.046	0.0097	-4.69	<.0001*
Amplitude x Amplitude	-0.049	0.0172	-2.83	0.0091*
Amplitude x Electrode size	-0.066	0.0129	-5.11	<.0001*
Amplitude	-0.08	0.0116	-7.66	<.0001*

G

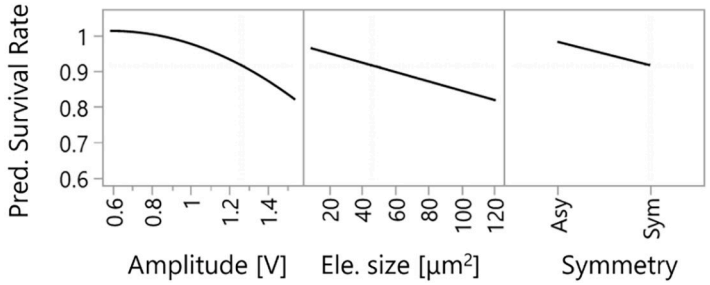

Fig. 6. Cytotoxicity screening experiment and corresponding linear regression model. A: Summary of the properties of the cell survival regression model. B: Analysis of variance of the cell survival model obtained by AICc minimization. C: Actual Survival Rate vs Survival Rate predicted by the regression model. The dashed curves represent the 0.05 significance curves. D and E: Confocal fluorescence microscopy images of cells electroporated in the presence of PI (D) and later stained for cell death with YO-PRO-1 (E). Cells that were electroporated and survived the process display only red fluorescence (white arrows), while the cells killed by electroporation show both red and green fluorescence (green arrows). F: Sorted estimates of the factors present in the cell survival model. G: Relationship between pulse amplitude, electrode size, pulse symmetry respectively and predicted cell survival rate. A detailed and interactive model is available in the supplementary materials. (For interpretation of the references to colour in this figure legend, the reader is referred to the web version of this article.)

impact, while they were reported to be contributing factors in explaining cell death [6]. The limited number of runs in which cell death did occur may provide only limited useful data points from which to build a linear regression model. On the positive side, the high survival rates observed during the screening experiment shows that electroporation on the HD-EP chip factors in a large range of useful parameters that can be tuned to optimize intracellular delivery without causing cell death.

2.5. Finding and applying optimized electroporation parameters

The two regression models built on dextran delivery and cell death data were used to find the values of electroporation parameters that would find the best compromise between maximal intracellular delivery and minimal cell death. These optimized electroporation conditions were 610 symmetric pulses with 1.22 V amplitude, 1.87 ms duration submitted to 45.5 μm^2 electrodes. This electrode size value had been fixed before optimization as it was the closest available to the optimal one suggested by the regression model (approximately 80 μm^2). Nonetheless, it is possible to select a different electrode size and find the corresponding optimal electroporation conditions. For instance, if single-cell electroporation is crucial, smaller electrodes could be chosen, and the other parameters would be increased in compensation. The amplitude of 1.22 V is the point above which cell viability drastically decreases and has been chosen by the maximization algorithm to reflect the high importance we set for the outcome "Survival Rate". On the other hand, the intermediate values chosen for duration and pulse number come from the constraints set between the parameters to generate the runs of the screening experiment (details in the Materials and Methods). In fact, according to the regression models, increasing the pulse duration should improve electroporation outcome. Combinations of high amplitudes and long durations, however, were not included in the screening experiments, and the maximization algorithm will not output parameter values that were not yet tested.

These optimal electroporation conditions were applied for the delivery of Cas9-GFP RNPs, a 70 kDa fluorescein-labelled dextran ("FD70") and of an mCherry-encoding mRNA. While we can in principle expect the delivery of those large molecules to require specific electroporation conditions, we hypothesized that the FD10-optimized parameters would be viable, but not optimal, to deliver large cargos and mRNA in cells. Our assumption is that maximizing the delivery of FD10 is an indirect

means of maximizing the formation of pores on the cell membrane during electroporation. As electroporation creates pores with sizes distributed over a large range (up to 50 nm[1]), maximizing the overall pore formation should also lead to an increase in pores large enough for entry of FD70 or Cas9 RNPs. In the different case of electrotransfection, the nucleic acids require electric fields to approach the cell membrane and interact with membrane pores formed during electroporation, before being internalized by the cell [22]. When performing electroporation on our MEA chip, biphasic pulses might not offer a net electrophoretic motion, but their anodic (positive) phase does provide an opportunity for the mRNA molecules to interact with membrane pores. Thus, electroporation parameters that maximize pore formation should also lead to a successful delivery of nucleic acids.

The results of these three experiments are presented in Fig. 7 (A-C). While the resulting fluorescence signal is faint but clearly detectable (Supplementary Fig. S3 D), the intracellular delivery of Cas9-GFP RNPs with the HD-EP chip is shown possible, opening the door to future gene editing applications. It is worth noting that the RNPs are much larger (200+ kDa) than the FD10 used to optimize the electroporation parameters, suggesting that maximizing the extent of electroporation can yield viable parameters for the delivery of large molecules. Cells electroporated in the presence of the large dextran molecule showed a more pronounced fluorescence signal (Fig. 7B). As multiple fluorophores are present on each dextran molecule, dextrans are intrinsically brighter than RNPs which contain a single GFP protein. The experiments prove that electroporation on microelectrode arrays can be used for the delivery of large biological molecules. Interestingly, large dextrans seemed to be excluded from the cell nucleus, while the FD10 were not (Fig. 7, D-G). This is consistent with the cut-off of 30 to 60 kDa that is often reported as the size limit above which diffusion through nuclear pore complexes is limited [23]. It may also indicate that the pulse parameters used in those experiments do not permeate the nucleus of the cells on the HD-EP chip, which can be desirable in some applications. On the other hand, RNPs contain a nuclear localization signal and did not seem excluded from the cell nucleus. Half of the electrodes resulted in successful delivery of FD70 or Cas9-GFP RNPs (ca. 50% efficiency) (Supplementary Fig. S3 A and B), which contrasts with the higher efficiency delivery of FD10. The size of the pores created by electroporation is notoriously small compared to other techniques [1] and delivering large, uncharged molecules is a more challenging task and might require more optimization [9]. Our RNP and FD70 delivery success of 50%, however, falls within the range of values reported for other techniques [12], and could most likely be improved with a dedicated optimization.

In the case of mRNA delivery, mCherry fluorescence could already be detected in some cells as early as an hour after electroporation (data not shown). Four hours after electroporation, the cells displayed clear fluorescence (Fig. 7C) and 13 out of the 16 active electrodes were in contact with a cell expressing mCherry (Supplementary Fig. S3 C), resulting in successful electrotransfection and expression of mRNA on >81% of the electrodes 4 h after electroporation. While cell death could not be monitored during this experiment, the regression model built during the cell survival analysis predicts a survival rate of 93% (±3%). An mRNA transfection efficiency above 80% and a survival rate above 90%, resulting in a yield of 74% (the yield being calculated as the

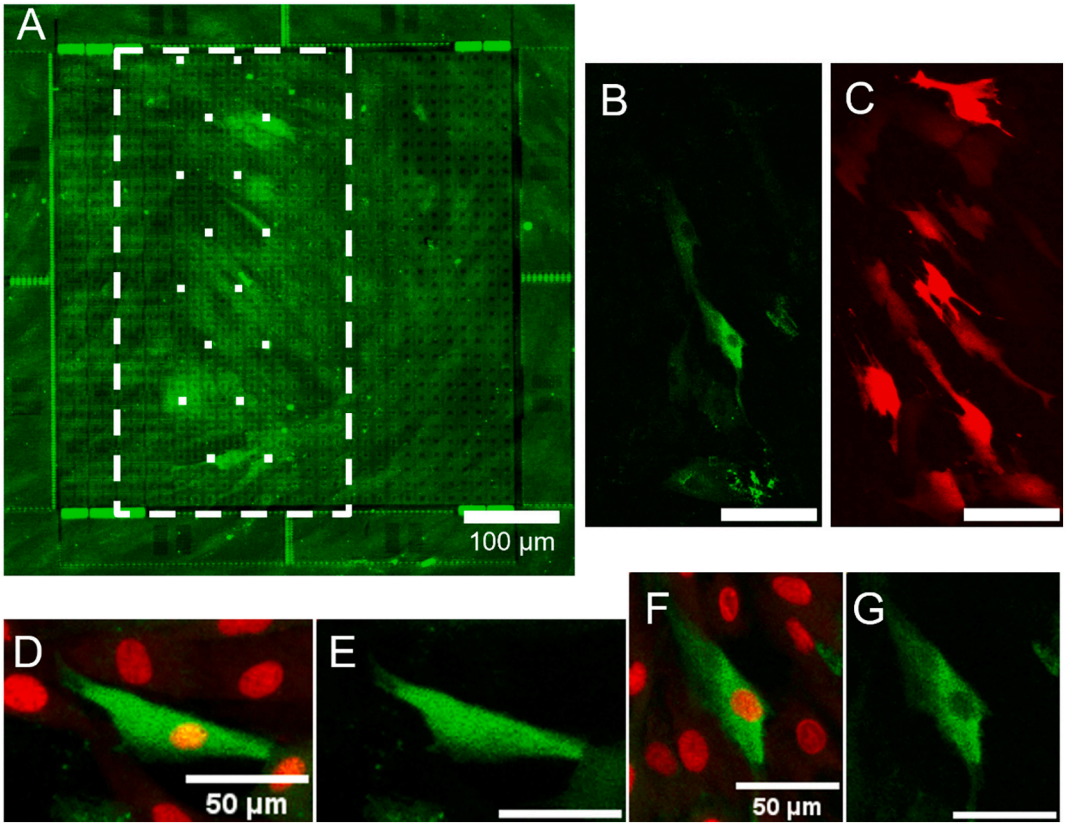

Fig. 7. Delivery of Cas9-GFP RNPs, dextran (70 kDa) and mCherry-encoding mRNA in primary human dermal fibroblasts with optimized electroporation conditions. A: Confocal fluorescence microscopy of the electrode cluster after delivery of Cas9-GFP RNPs. The dashed rectangle outlines the area displayed in panels B and C. The area is centered around the 45.5 mm^2 electrodes, which was the optimal electrode size used to deliver the large molecules while maximizing cell survival. The 16 white squares represent the electrodes activated for electroporation. B: Confocal fluorescence microscopy of cells after delivery of FD70. C: Cells transfected with mCherry-encoding mRNA, imaged four hours after electroporation. B and C: Scalebar is 100 µm. D-G: Examples of cells electroporated either in presence of FD10 (D, E) or FD70 (F, G). Cell nuclei are stained with SYTO 61 (red). The 10 kDa dextran can diffuse freely in the nucleus of cells and their cytosol is homogeneously fluorescent (E), while 70 kDa dextrans are excluded from the nucleus, leaving a dark spot in the middle of the cell (G). (For interpretation of the references to colour in this figure legend, the reader is referred to the web version of this article.)

product of cell survival and transfection efficiency), puts HD-EP performance above values reported for commercial electroporators in primary cells [24] and on par with the most effective single-cell transfection technologies [12]. As a point of comparison, performing the transfection of primary fibroblasts on a commercial electroporator resulted in approximately 60% of cell viability (Supplementary materials and methods and Supplementary Fig. S4), and almost all the surviving cells expressed mCherry after 6 h, resulting in a yield of 60%. Many cells, however, showed round morphology uncharacteristic of healthy adherent cells, further suggesting long lasting disruption of cell functions for the cells that did survive.

This showcases the possibility to perform a highly efficient, spatially resolved transfection on the HD-EP chip. As for the delivery of small and large dextrans, mRNA transfection still gives rise to a large cell-to-cell variability in fluorescence intensity. After two days of incubation, however, the fluorescent cells had spread across the electrode cluster and did not match the locations of the electrodes active during electroporation (See Supplementary Fig. S3 E).

3. Conclusion

Thanks to the multiplexing ability of the CMOS HD-EP chip, we designed and implemented a quick and efficient workflow to transfect individual cells in a human dermal fibroblast culture with high efficiency and precision. Regression models fitted to the data on dextran delivery and cell death were largely in agreement with previous literature and could be used to predict the outcome of untested electroporation conditions. We also demonstrated that intracellular delivery of molecules happened at values of electroporation parameters much lower than values that caused cell death. For more insightful follow-up studies on cell death in the context of electroporation, it would be recommended to use a different screening experiment, that investigates a larger range of values of electroporation parameters than the ones used to investigate delivery. Thanks to the regression models, electroporation conditions to maximize electroporation and minimize cell death were generated and applied to the delivery of Cas9-GFP RNPs, 70 kDa dextran and an mCherry-encoding mRNA. Delivery of the mRNA resulted in successful transfection on >80% of the electrodes used for electroporation, with a predicted cell survival rate above 90%. The higher yield obtained on our HD-EP chip, combined with its multiplexing/spatially resolved electroporation abilities, make it an ideal platform to implement certain screening applications that we detail at the end of text. However, the use of adherent cells render it inherently lower throughput compared to in-flow transfection methods such as in-flow electroporation or microfluidic cell squeezing, which are preferable to produce modified cells in large scales but less amenable to screening experiments.

Interestingly, optimized electroporation parameters used in transfection experiments were deducted from observations made on the delivery of a small molecule. While the delivery of small molecules relies on different mechanisms of intracellular entry than larger, charged molecules like mRNA, it could be expected that these different molecules would require distinct pulse parameters. These promising results, however, show that optimizing electroporation itself (as quantified by the uptake of small molecules) is an efficient, cargo agnostic method to generate electroporation conditions for the delivery of larger, more challenging molecules. The conditions found in this way may not be optimal for a specific molecule but might be viable for many others, like in the case of larger dextrans and mRNA. Moreover, in the case of a molecule that may require its own delivery optimization or dosage control, the workflow that we showcased in this study can quickly and conveniently generate electroporation conditions that maximize delivery efficiency and cell survival. Finally, future work should also focus on including more complex electroporation strategies to the screening experiments. For instance, implementing on chip elegant electroporation conditions combining pulses of different amplitudes and durations to achieve a net movement of molecules toward the cells [6] could further improve the efficiency of HD-EP. A tailored HD-EP CMOS chip that can host larger amounts of cells while keeping single cell precision might be an advantage for moving this to practical applications.

We believe that HD-EP will drive forward drug screening applications relying on the intracellular delivery of a large library of biologically active compounds. For instance, the cytotoxic activity of chemotherapeutic drugs can be enhanced up to thousand-fold upon cellular entry through electroporation, a process known as electrochemotherapy [25]. By sequentially introducing different cargos to cancer cells grown on our HD-EP chip, and by activating only a subset of electrodes at a time, the electrochemotherapeutic activity of different drugs could be tested at different locations of the chip in parallel. The addition of a microfluidic system to automate the drug dispensing will result in a fast and highly parallelized drug screening platform [26]. The small number of cells present on the chip during HD-EP (~50,000) would make this technique amenable to patient-derived tumour samples, paving the way to a fast and personalized treatment selection. Another application that is well served by HD-EP is the creation of so-called organs-on-a-chip for in vitro drug testing. That is, the spatially resolved transfection and differentiation of patient-derived stem cells will allow the creation of tissues with a physiologically relevant architecture, a step toward more predictive disease models and clinical trials in a dish [27]. Moreover, the monitoring abilities of the HD-EP chip would generate label-free, real-time data about the tested drugs' effectiveness at the single cell level.

4. Materials and methods

In this work, we used 32 different electroporation conditions in which four pulse train parameters and the electrode size are varied to optimize the electroporation efficiency and cell survival (Fig. 8A). All those distinct electroporation conditions were tested in parallel in a single experiment by submitting them to different locations of the active area on our CMOS HD-EP chip (Fig. 8D). The 32-run experiment was performed twice: once to evaluate the impact that the electroporation parameters have on the intracellular delivery of small molecules, and another time to evaluate their impact on cell survival.

4.1. CMOS HD-EP Chip and spatially resolved electroporation

The CMOS MEA chip fabrication and packaging have been described in Mora Lopez et al. (2018) [16] and Miccoli et al. (2019) [15], respectively. While the device features 6 different cell interfacing modalities, including electrophysiological recording and impedance monitoring, this work focuses on its voltage stimulation abilities, that were used to electroporate and transfect adherent cells grown on the active area of the chip. The 5×5 mm^2 active area of the HD-EP chip comprises 16,384 individually addressable titanium nitride (TiN) microelectrodes with sizes of 2.5×3.5, 4.5×4.5, 6.5×7, 11×11 (8.75, 20.25, 45.5 and 121) mm^2. Those electrodes are distributed across 16 clusters arranged into a 4 by 4 matrix, and each cluster forms a grid of $32 \times 32 = 1024$ electrodes with 15 μm pitch between electrodes. Every electrode is connected to a stimulation unit comprising a 5-bit digital-to-analog (DAC) converter and can be individually selected to submit voltage pulses of up to ±1.65 V. Around each cluster, eight additional large (235×50 μm^2) electrodes were patterned to serve as references (Fig. 1B). The HD-EP chip was plugged into an in-house developed benchtop setup. That setup had the two roles of powering the chip and connecting it to a computer running a custom-made configuration software. In the configuration software, the user can select spatial patterns of electrodes and design square-wave voltage pulse trains that will be sent to the selected electrodes.

We used the ability to individually address the microelectrodes to submit the different electroporation pulse trains designed by DoE to different locations of the HD-EP chip's active area, effectively

A

Parameter	Role	Low Level	High Level
Amplitude [V]	Continuous	0.5	1.5
Duration [ms]	Continuous	0.5	3
Pulse number	Continuous	250	750
Pulse symmetry	Categorical	Asymmetric	Symmetric
Electrode size [μm^2]	Continuous	8.75	121

B

Amplitude*Amplitude	Duration*Duration	Pulse number*Electrode size
Amplitude*Duration	Duration*Pulse Number	Pulse number*Symmetry
Amplitude*Pulse number	Duration*Electrode size	Electrode size*Electrode size
Amplitude*Electrode size	Duration*Symmetry	Electrode size*Symmetry
Amplitude*Symmetry	Pulse number*Pulse number	Blocking factor

C

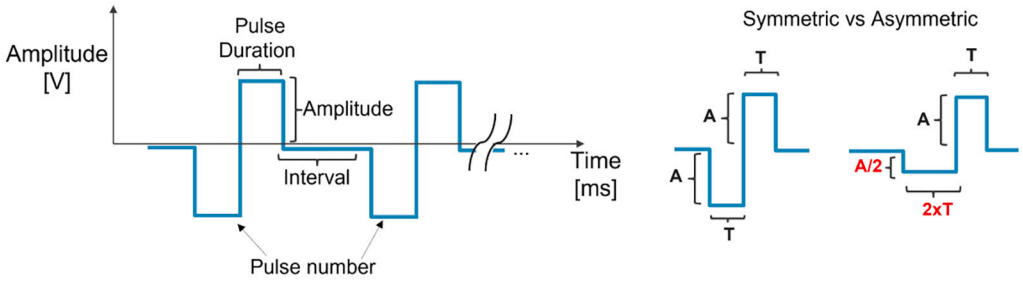

D

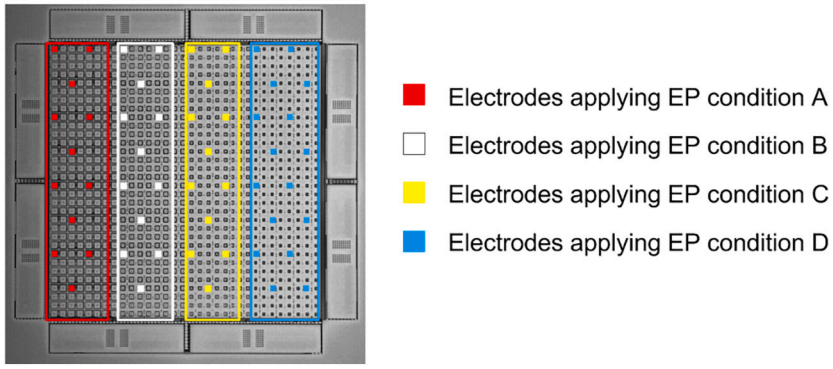

Fig. 8. Summary of the implementation of the multiplexed, on-chip electroporation screening experiment. A: Table listing the five electroporation parameters evaluated in the screening experiment designed with DoE, along the range of values in which they varied in the different runs. B: List of quadratic and interaction effects evaluated in the screening experiments in addition to the main effects presented in A. A blocking factor has been added to take into consideration potential differences between the two chips used in parallel to perform the screening experiment. An intercept also must be estimated, bringing the total number of terms in the model to 21. C: Example of a generic pulse train showing the parameters evaluated in the screening experiment. The pulse interval was not included in the DoE and kept constant at 1 ms. D: To perform multiple runs simultaneously in different areas of the HD-EP chip, 4 electrodes clusters have been divided into four compartments, outlined with different colors. Each compartment had a different electrode size. In each compartment, 12 to 16 electrodes (represented by colored squares) have been selected to submit an electrical stimulation. Gaps where no electrodes were activated were left in between compartments to avoid cells spanning across compartments and being stimulated with multiple electroporation conditions. It resulted in most compartments comprising 12 active electrodes (red, white, and yellow), except for the rightmost compartments that comprise 16 (blue). To perform 32 different electroporation conditions in parallel, two chips were used at the same time, each performing 16 runs. (For interpretation of the references to colour in this figure legend, the reader is referred to the web version of this article.)

multiplying the number of electroporation conditions tested in a single experiment. More precisely, each electrode cluster was split into four regions of a single electrode size, effectively dividing the active area into different "experimental compartments", in which a distinct electroporation pulse train can be tested. To observe the electroporation of single-cells and prevent cells from being stimulated by multiple electrodes at once, a set of 12 or 16 evenly spaced electrodes per compartment were selected to submit a common electroporation pulse train (they are referred to as the active electrodes). That is, most microelectrodes remained idle and only a few were active during the electroporation sequence. A gap of idle electrodes was left between compartments to prevent cells from being electroporated with two electroporation conditions at once. It resulted in most compartments comprising 12 active electrodes, except for the rightmost compartments that comprise 16 (Fig. 8D, shown by colored squares).

4.2. Explored electroporation parameters

In this work, we evaluate the effects of five electroporation parameters: the electrode size and four pulse parameters. All the electroporation pulses tested were cathodic-leading, balanced biphasic voltage pulses. There was a 1 ms interval between pulses. The pulse parameters that were investigated in this study are the pulse amplitude, the positive phase duration (referred to as pulse duration), the number of pulses and the pulse symmetry (Fig. 8A). In symmetric pulses, the negative phase had the same duration and amplitude as the positive phase, while in asymmetric pulses the negative phase had half the amplitude but twice the duration of the positive phase (Fig. 8C).

The "Custom Design" function of the software JMP® (Version *15*. SAS Institute Inc., Cary, NC, 1989–2021) was used to generate 32 different electroporation conditions (see Supplementary Table 2), designed to predict the effects that five factors (four electroporation pulse parameters plus the electrode size) have on two response parameters. The first response is the average fluorescence intensity of the cells after electroporation with a fluorescently labelled cargo, that we use as a quantification of the amount of molecule delivered in the cells. The second response is the survival rate, calculated from the ratio of dead and apoptotic cells to electroporated cells, that gives us a measure of the electroporation conditions' cytotoxicity. The goal for those two responses was set as maximize.

The five factors investigated, with their low and high levels, are shown in Fig. 8A. Standard coding was applied to the quantitative factors. Because the active area of the chip has been divided in different experimental compartments each comprising electrodes of a single fixed size, the electrode size was defined as a covariate factor. The range of values for the parameters tested was defined according to preliminary results and was chosen to limit cell death. A 21-term model was generated by including all the main (5 terms) and quadratic effects (4 terms, the quadratic effect of pulse symmetry, a categorical factor, cannot be evaluated), all two-way interactions of the five factors (10 terms), an intercept and a blocking factor (2 terms) (Fig. 8B). Moreover, to avoid the cell death resulting from exposure to strong electroporation conditions, two linear constraints were implemented to avoid the generation of runs with combinations of high amplitude and long duration, or of long duration and large pulse numbers (see Supplementary Table 3).

As only four of the electrode clusters on the HD-EP chip contain each of the electrode sizes of interest for this study, the full DoE had to be performed on two separate chips, used at the same time. The 32 runs were thus split in two blocks of 16 runs each, corresponding to the two different chips used. The blocking factor was introduced to detect any change in results due to variations in fabrication or handling of the chips. Fig. 8A and B show the full list of terms investigated in the DoE.

The design was made I-Optimal, as these designs are well suited for predicting and optimizing the modelled processes [28]. In the 32 different electroporation conditions designed by JMP, the pulse amplitudes of the runs were slightly adjusted to match the closest value available in the stimulation unit's 5-bit DAC.

4.3. Culture of human dermal fibroblasts

Neonatal human Dermal Fibroblasts (HDF, ATCC PCS-201-010) cells were obtained from the American Type Culture Collection (ATCC) and are a common cell type displaying the typical features of primary cells such as limited proliferation and transfection efficiency with standard methods compared to immortalized cell lines. They are of use for the generation of induced pluripotent stem cells through delivery of reprogramming genes and gene editing experiments. They were cultured in a standard cell culture incubator (37 °C, 100% humidity, 5% CO_2) in Dulbecco's modified Eagle's medium/Nutrient mixture F12 with GlutaMAX supplement (DMEM/F12, Gibco™), augmented with 10% foetal bovine serum (FBS, Gibco™) and 1% Penicillin-Streptomycin (10,000 U/ml, Gibco™). Cells were passaged every two to three days with 0.05% trypsin-ethylenediaminetetraacetic (EDTA, Gibco™) and were discarded after ten passages.

4.4. Culture of cells on the CMOS HD-EP chip

To prepare the CMOS HD-EP chip for cell culture, the central wall of a Culture-Insert 2 Well for wound healing assay (IBIDI) was cut away and the insert was glued around the active area of the chip with a biocompatible epoxy resin (EPO-TEK® 353ND, Epoxy Technology). The chip's active area was then sterilized with 70% ethanol for 5 min and rinsed three times with sterile high purity water (HPW).

In between experiments, the chip was cleaned by depositing a 1% *w/v* solution of Tergazyme® (Alconox®, Sigma-Aldrich) in the culture insert and incubating it at 37 °C for 20 min. The chip was then abundantly rinsed with HPW and resterilised.

After reaching approximately 80% confluency, HDF cells were detached from the culture flasks with 0.05% Trypsin-EDTA, counted with a Countess 2 FL Automated Cell Counter (Countess 2, Invitrogen) and resuspended in DMEM/F12 at a concentration of 1.2×10^5 cells/ml. 250 µl of cell suspension (30,000 cells, for a density of about 43,000 cells/cm^2) were deposited in the insert on the chip. To obtain a homogeneous cell density across the chip surface, the chip was put on a vibration free surface for 30 min to let the cells settle [29]. The chip was then put in a cell culture incubator for approximately 36 h.

4.5. Electroporation of cells on the CMOS HD-EP chip

All the electroporation experiments were performed at room temperature, approximately 30 h after the cells were seeded onto the CMOS HD-EP chip. The molecules to be delivered in the cells through electroporation were all dissolved in phenol red-free Hank's Balanced Salt Solution containing Calcium and Magnesium (HBSS, Gibco™). The dextrans were dissolved at a concentration of 4 mg/ml in HBSS. The Cas9-GFP RNPs were first assembled by mixing 4 µl of Cas9-GFP Protein reconstituted in nuclease free water with glycerol at a concentration of 50 µM (Sigma-Aldrich) and 4 µl single-guide RNA (Integrated DNA Technologies) reconstituted in Tris-EDTA at a concentration of 200 µM. After 10 min incubation at room temperature, the RNP mix was added to 32 µl of HBSS, with a final Cas9 concentration of 5 µM.

Before the dextran or RNP delivery experiments, the CMOS HD-EP chip was connected to the control setup. Then, the culture medium was removed and replaced with either 50 µl of a solution of fluorescein-labelled dextrans 10 kDa (FD10, Invitrogen) or 70 kDa (FD70, Invitrogen), or 40 µl of a solution of RNPs. The cargo solutions were left in contact with the cells for two minutes before the electroporation sequence was triggered. After the end of the final electroporation step, the cells were incubated with the dextran solution for two more minutes. Finally, the solution was removed, and the culture insert was gently rinsed three times with 250 µl of warm HBSS. After the last rinsing step, the cells were stained with 200 µl of HBSS containing the red nucleic acid stain SYTO 61 (Molecular Probes) at a concentration of 2.5 µM. After 20 min of incubation in a cell culture incubator, the dye solution was replaced with HBSS, and the cells imaged.

For the cytotoxicity experiment, the CMOS HD-EP chip was connected to the control setup and the culture medium replaced with a solution of Propidium Iodide (PI, Molecular Probes) dissolved at a concentration of 100 µg/ml in HBSS. The electroporation sequence was triggered after two minutes of incubation, and the cells were incubated for 10 min with PI. Then, the apoptosis and cell death indicator YO-PRO™-1 Iodide (YO-PRO-1, Invitrogen) was added to the solution to reach 1 µM, and the nuclear stain Hoechst 34580 (BD Pharmingen) was added for a final concentration of 2 µg/ml. The cells were incubated with the dyes for 30 min and imaged.

For the transfection experiments, mRNA encoding the fluorescent protein mCherry (CleanCap® mCherry mRNA (5moU), Trilink

Biotechnologies) was diluted in HBSS at a concentration of 50 μg/ml. The culture medium in the insert was first removed, and the active area of the CMOS HD-EP chip was gently rinsed once with 250 μl HBSS. Then, 50 μl of mRNA solution was applied to the cells and incubated for two minutes before the electroporation protocol was started, and for two more minutes after the end of the electroporation sequence. The nucleic acid solution was then removed from the insert and replaced with 250 μl of culture medium. The chip was put back in the cell culture incubator until further imaging of fluorescent protein expression. The cells were then imaged at multiple time points after transfection.

4.6. Fluorescence imaging and image analysis

Before imaging, the culture insert was covered with a glass coverslip. All the fluorescence microscopy was performed with a Zeiss Laser Scanning Microscope 780 confocal microscope and an EC "Plan-Neofluar" 10×/0.30 objective. The images were acquired sequentially. Fluorescein dextrans were imaged with standard GFP filter sets and excited with 488 nm light source. SYTO 61 was excited with 633 nm laser and imaged with a standard Cy5 filter. Hoechst 34580 was illuminated with a 405 nm light source and imaged with a custom filter set accepting light between 410 nm and 490 nm. The image processing and the extraction of cell fluorescence intensities were performed with FiJi [30] and Stardist [31]. The detailed workflow is presented in the Supplementary Material.

4.7. Data analysis of efficiency of electroporation

For each experimental run, the average fluorescence intensity of the cells after electroporation was measured and reported in JMP®. The fluorescence value for runs in which no fluorescent cell could be detected was set as 0. At first, the relationship between each data point y_i (the average cellular fluorescence intensity after electroporation) and the electroporation parameters x_j was assumed to follow the equation

$$y_i = \beta_0 + \sum_{j=1}^{n} \beta_j x_{ji} + \sum_{k=1}^{n-1} \sum_{j=k+1}^{n} \beta_{kj} x_{ki} x_{ji} + \sum_{j=1}^{n} \beta_{jj} x_{ji}^2 + b_\iota + e_\iota$$

In which a response y_i is modelled as the sum of a constant β_0, the main effects x_j and a blocking factor b_ι,all two term interactions $x_k x_j$, all quadratic terms x_j^2,and an error e_i. β_j, β_{kj} and β_{jj} are regression coefficients. This full model thus contains 21 terms: an intercept, a blocking factor, 5 main effects, 4 quadratic effects and 10 interactions.

Using JMP's "fit model" function, a backward, stepwise regression was performed to find the significant terms within the 21-term model evaluated in the DoE. The term selection rules were set as "Combine". Both minimum Bayesian Information Criterion (BIC) and minimum corrected Akaike Information Criterion (AICc) were used as a stopping rule. The coefficient of determination (R^2) adjusted coefficient of determination (aR^2) and the predicted residual error sum of squares (PRESS) were evaluated to find the better of the two models.

4.8. Validation of the JMP model

As a way of validating the resulting BIC model, three sets of electroporation parameters were generated, designed to produce specific fluorescence intensities within a cell after intracellular FD10 delivery through electroporation on our HD-EP chip. The prediction profiler function was used to define three electroporation parameter sets, designed to obtain cells with a fluorescence intensity of 5000 A.U., 10,000 A.U. and 15,000 A.U. Those electroporation conditions were tested in a validation dextran delivery experiment using the same protocol as for the screening experiment.

4.9. Data analysis of cytotoxicity of electroporation

For each experimental run, PI positive cells and YO-PRO1 positive cells were manually counted. Cell survival was quantified as the ratio of dead or dying cells to electroporated cells, and the nuclear stain H34580 was used to facilitate counting cells touching each other. Survival was calculated as Survival = 1 - (#YO-PRO1 cells / #PI cells). As for the dextran delivery experiments, two regression models were generated in JMP using a backward stepwise regression minimizing either the BIC or the AICc. In addition to R^2, aR^2 and PRESS, the physical relevance of the two models was used to decide which one was better.

4.10. Finding optimal electroporation parameters

After fitting two different models to the dextran delivery data and the cell survival data, the prediction formulas of those models were imported into JMP's profiler tool. Both outcomes were set as equally important but, to put a larger emphasis on cell survival, the associated desirability was set as 0 for a Survival of 0.5, desirability of 0.5 for a Survival of 0.75, and a desirability of 1 for a Survival of 1. The desirability function associated to dextran delivery was not modified. Before searching for the optimal parameters, the electrode size was locked at 45.5 μm^2, which was the closest size available to the optimal electrode found by the dextran delivery model. It should be noted that the electroporation conditions that can be obtained this way are not unique and running the maximization multiple times can lead to different optimal conditions.

Data availability

DoE table with fluorescence and cell viability data, and regression models available in the supplementary materials.

Acknowledgements

Bastien Duckert is SB PhD fellow at FWO with grant 1S84919N.

We thank Olga Krylychkina and Dennis Lambrechts for the fruitful discussions on cell culture and transfection protocols, Saeedeh Ebrahimi Takalloo for the discussions on electrochemistry principles, and Sarah Libbrecht and Wiebe Vanhove for the help provided in obtaining and analysing flow cytometry data.

Appendix A. Supplementary data, figures and methods

Supplementary data to this article can be found online at https://doi.org/10.1016/j.jconrel.2022.10.001.

References

[1] M.P. Stewart, R. Langer, K.F. Jensen, Intracellular delivery by membrane disruption: mechanisms, strategies, and concepts, Chem. Rev. 118 (2018) 7409–7531.
[2] S. Kar, et al., Single-cell electroporation: current trends, applications and future prospects, J. Micromech. Microeng. (2018), https://doi.org/10.1088/1361-6439/aae5ae.
[3] L. Chang, et al., Micro−/nanoscale electroporation, Lab Chip 16 (2016) 4047–4062.
[4] T. DiTommaso, et al., Cell engineering with microfluidic squeezing preserves functionality of primary immune cells in vivo, Proc. Natl. Acad. Sci. 115 (2018). E10907–E10914.
[5] M. Zhang, et al., The impact of Nucleofection® on the activation state of primary human CD4 T cells, J. Immunol. Methods 408 (2014) 123–131.
[6] M.M. Sadik, et al., Scaling relationship and optimization of double-pulse electroporation, Biophys. J. 106 (2014) 801–812.
[7] H.Y. Wang, C. Lu, Electroporation of mammalian cells in a microfluidic channel with geometric variation, Anal. Chem. 78 (2006) 5158–5164.
[8] A. Sharei, et al., A vector-free microfluidic platform for intracellular delivery, Proc. Natl. Acad. Sci. U. S. A. 110 (2013) 2082–2087.
[9] H. He, D.C. Chang, Y.K. Lee, Using a micro electroporation chip to determine the optimal physical parameters in the uptake of biomolecules in HeLa cells, Bioelectrochemistry 70 (2007) 363–368.

[10] T. Geng, et al., Flow-through electroporation based on constant voltage for large-volume transfection of cells, J. Control. Release 144 (2010) 91–100.
[11] M.P. Stewart, et al., In vitro and ex vivo strategies for intracellular delivery, Nature 538 (2016) 183–192.
[12] B. Duckert, S. Vinkx, D. Braeken, M. Fauvart, Single-cell transfection technologies for cell therapies and gene editing, J. Control. Release (2020), https://doi.org/10.1016/j.jconrel.2020.10.068.
[13] R. Xiong, et al., Photothermal nanofibres enable safe engineering of therapeutic cells, Nat. Nanotechnol. 16 (2021) 1281–1291.
[14] A. Tay, N. Melosh, Transfection with nanostructure electro-injection is minimally perturbative, Adv. Ther. 1900133 (2019), 1900133.
[15] B. Miccoli, et al., High-density electrical recording and impedance imaging with a multi-modal CMOS multi-electrode array chip, Front. Neurosci. 13 (2019) 1–14.
[16] C.M. Lopez, et al., A multimodal CMOS MEA for high-throughput intracellular action potential measurements and impedance spectroscopy in drug-screening applications, IEEE J. Solid State Circuits 53 (2018) 3076–3086.
[17] J. Kuha, AIC and BIC, Sociol. Methods Res. 33 (2004) 188–229.
[18] J. Gehl, Electroporation: theory and methods, perspectives for drug delivery, gene therapy and research, Acta Physiol. Scand. 177 (2003) 437–447.
[19] S.F. Cogan, Neural stimulation and recording electrodes, Annu. Rev. Biomed. Eng. 10 (2008) 275–309.
[20] N. Pour Aryan, H. Kaim, A. Rothermel, Stimulation and Recording Electrodes for Neural Prostheses 78, Springer International Publishing, 2015.
[21] P.E. Boukany, et al., Nanochannel electroporation delivers precise amounts of biomolecules into living cells, Nat. Nanotechnol. 6 (2011) 747–754.
[22] C. Rosazza, S. Haberl Meglic, A. Zumbusch, M.-P. Rols, D. Miklavcic, Gene Electrotransfer: a mechanistic perspective, Curr. Gene Ther. 16 (2016) 98–129.
[23] B.L. Timney, et al., Simple rules for passive diffusion through the nuclear pore complex, J. Cell Biol. 215 (2016) 57–76.
[24] H.G. Dixit, et al., Massively-parallelized, deterministic mechanoporation for intracellular delivery, Nano Lett. (2019), https://doi.org/10.1021/acs.nanolett.9b03175.
[25] U. Probst, I. Fuhrmann, L. Beyer, P. Wiggermann, Electrochemotherapy as a new modality in interventional oncology: a review, Technol. Cancer Res. Treat. 17 (2018), 153303381878532.
[26] T. Pauwelyn, et al., High-throughput CMOS MEA system with integrated microfluidics for cardiotoxicity studies, Front. Cell. Neurosci. 12 (2018).
[27] B. Miccoli, D. Braeken, Y.-C.E. Li, Brain-on-a-chip devices for drug screening and disease modeling applications, Curr. Pharm. Des. (2019), https://doi.org/10.2174/1381612825666190220161254.
[28] P. Goos, B. Jones, U. Syafitri, I-optimal design of mixture experiments, J. Am. Stat. Assoc. 111 (2016) 899–911.
[29] Z. Wang, J.M. Belovich, A simple apparatus for measuring cell settling velocity, Biotechnol. Prog. 26 (2010) 1361–1366.
[30] J. Schindelin, et al., Fiji: an open-source platform for biological-image analysis, Nat. Methods 9 (2012) 676–682.
[31] U. Schmidt, M. Weigert, C. Broaddus, G. Myers, Cell Detection with Star-Convex Polygons, 2018, pp. 265–273, https://doi.org/10.1007/978-3-030-00934-2_30.